Raman scattering from molecular conduction junctions: Charge transfer mechanism

Michal Oren,[1,*] Michael Galperin,[2,†] and Abraham Nitzan[3,‡]
[1]*School of Physics, Tel Aviv University, Tel Aviv, 69978, Israel*
[2]*Department of Chemistry and Biochemistry, University of California at San Diego, La Jolla, California 92093, USA*
[3]*School of Chemistry, Tel Aviv University, Tel Aviv, 69978, Israel*
(Received 12 January 2012; published 26 March 2012)

We present a model for the charge transfer contribution to surface-enhanced Raman spectroscopy (SERS) in a molecular junction. The model is a generalization of the equilibrium scheme for SERS of a molecule adsorbed on a metal surface [B. N. J. Persson. Chem. Phys. Lett. **82**, 561 (1981)]. We extend the same physical consideration to a nonequilibrium situation in a biased molecular junction and to nonzero temperatures. Two approaches are considered and compared: a semiclassical approach appropriate for nonresonance Raman scattering, and a quantum approach based on the nonequilibrium Green's function method. Nonequilibrium effects on this contribution to SERS are demonstrated with numerical examples. It is shown that the semiclassical approach provides an excellent approximation to the full quantum calculation as long as the molecular electronic state is outside the Fermi window, that is, as long as the field-induced charge transfer is small.

DOI: 10.1103/PhysRevB.85.115435 PACS number(s): 73.23.−b, 78.20.Jq, 78.30.−j, 78.67.−n

I. INTRODUCTION

Single-molecule Raman spectroscopy is by now a well-established field of research, where surface enhancement of the signal makes experimental observation feasible.[1,2] Recent advances in fabricating molecular junctions[3] have made it possible to observe surface-enhanced molecular optical response of such systems under nonequilibrium current-carrying conditions.[4–6] In particular, surface-enhanced Raman spectroscopy (SERS) of molecular junctions has the potential to become an important diagnostic and control tool in the field of molecular electronics. Together with inelastic electron tunneling spectroscopy,[7–9] it can provide detailed information on the vibrational structure (molecular fingerprint) and dynamical effects of a junction. SERS also is an invaluable source of information on vibrational energy distribution in a molecular junction.[6,10]

Development of experimental techniques has led to a surge in theoretical research on spectroscopy of nonequilibrium open molecular systems. Theoretical studies on current-induced fluorescence[11–15] and photoassisted current[16–19] are available in the literature. Recently, we[20,21] proposed an approach for describing resonant Raman spectroscopy of molecular conduction junction within a two-level (HOMO-LUMO) model for the molecular bridge. With many experiments done far from resonance, a natural extension is the formulation of a theory for off-resonant Raman scattering. Another important extension is to address the often raised issue of the so-called "chemical" contribution, a name usually referred to as charge transfer (CT) effect to SERS in such systems. The issue is particularly relevant in molecular junctions, where CT is significantly expressed in their behavior under bias.

Many studies aimed to characterize the role played by CT in SERS from molecules adsorbed on metal surfaces have been published in the past three decades.[22–29] A particularly simple model by Persson[30] considers the light-scattering signal resulting from the oscillating dipole formed by CT between an adsorbed molecule and the underline metal as evaluated within a Newns-Anderson–type model.[31] In this paper, we extend this theory to a molecule confined between the two metal electrodes of a biased molecular junction. We use a nonequilibrium Green's function (NEGF) technique to calculate the light scattering from such systems and identify diagrams on the Keldysh contour that contribute to the charge transfer SERS. We derive an expression for the Raman flux at steady state, thus generalizing the theory of Ref. 30 to nonzero temperature and current-carrying conditions. Our results become identical to those of Ref. 30 in the equilibrium zero-temperature limit.

The problem of Raman scattering from a molecule in a metal-molecule-metal junction is associated with two fundamental issues. One is the electromagnetic response of the junction, specifically, one needs to relate the incident electromagnetic field to the local field in the junction as well as outgoing radiation to the time-dependent charge distribution in the junction. The other is the evaluation of the transport properties of the junction and the time-dependent charge distribution in the junction in the presence of the combined driving by the dc voltage bias and the local time-dependent electromagnetic field. Here, we focus on the second problem, assuming that the electromagnetic response of the junction has been (or can be) evaluated in a separate calculation. Such an approach has been tacitly followed in most treatments of radiation field effects on electronic transport in tunneling junctions. Several recent calculations[15,32] have addressed the needed input using numerical solutions of the Maxwell equations in an environment defined by a given junction geometry.

Our model is introduced in Sec. II. A quasiclassical approach to CT contributions to SERS is discussed in Sec. III. Section IV introduces corresponding quantum consideration and identifies the Keldysh contour diagrams for the light-scattering process relevant to obtain the CT contributions to SERS. Numerical examples are presented in Sec. V, and our conclusions are summarized in Sec. VI.

II. MODEL

Following Ref. 30, the molecular junction is represented by a single level of energy ε_0 coupled to two metal contacts L and

R, each at its own equilibrium characterized by the junction temperature T and the electrochemical potentials $\mu_L = E_F + \eta|e|V_{sd}$ and $\mu_R = E_F - (1-\eta)|e|V_{sd}$, respectively, where V_{sd} is the potential bias and where the bias division factor η is used to model the voltage distribution in the junction. The tunneling electron is coupled to a single molecular vibration of frequency ω_v, which in turn is coupled to a thermal bath of harmonic oscillators. In addition to the imposed bias, the junction is driven by an external field represented by a single pumping mode of frequency ν_i and a continuum of modes $\{\nu_f\}$ that are assumed vacant. The light-scattering signal is calculated as the flux into the latter modes.

In the absence of the electromagnetic field, the system Hamiltonian is

$$\hat{H} = \hat{H}_0 + \hat{V}, \tag{1}$$

$$\hat{H}_0 = \hat{H}_M + \sum_{K=\{L,R,B\}} \hat{H}_K, \tag{2}$$

$$\hat{V} = \hat{V}_M + \sum_{K=\{L,R,B\}} \hat{V}_{MK}, \tag{3}$$

where $\hat{H}_M$ is the molecular Hamiltonian that describes the electronic and vibrational degrees of freedom of the molecule

$$\hat{H}_M = \varepsilon_0 \hat{n} + \omega_v \hat{v}^\dagger \hat{v} \tag{4}$$

and $\hat{H}_K$ ($K = \{L,R,B\}$) are Hamiltonians of the electrodes (L and R) and thermal bath (B):

$$\hat{H}_K = \sum_{k\in K} \varepsilon_k \hat{c}_k^\dagger \hat{c}_k, \tag{5}$$

$$\hat{H}_B = \sum_\beta \omega_\beta \hat{b}_\beta^\dagger \hat{b}_\beta. \tag{6}$$

$\hat{V}_M$ is the coupling between the molecular electronic and vibrational degrees of freedom, and $\hat{V}_{MK}$ ($K = L,R,B$) are couplings between molecule and corresponding bath:

$$\hat{V}_M = M_v(\hat{v} + \hat{v}^\dagger)\hat{n}, \tag{7}$$

$$\hat{V}_{MK} = \sum_{k\in K}(V_k \hat{d}^\dagger \hat{c}_k + V_k^* \hat{c}_k^\dagger \hat{d}), \qquad K = L,R \tag{8}$$

$$\hat{V}_{MB} = \sum_\beta W_\beta \hat{Q}_\beta \hat{Q}_v. \tag{9}$$

In Eqs. (4)–(9), $\hat{d}^\dagger$ ($\hat{d}$) and $\hat{c}_k^\dagger$ ($\hat{c}_k$) are creation (annihilation) operators for electrons on the molecule and in state k of the contacts, $\hat{n} \equiv \hat{d}^\dagger \hat{d}$ is the population operator of the molecular level, $\hat{v}^\dagger$ ($\hat{v}$) and $\hat{b}_\beta^\dagger$ ($\hat{b}_\beta$) are creation (annihilation) operators of vibrational excitation (phonon) on the molecule and in state β of thermal bath, $\hat{Q}_v \equiv \hat{v} + \hat{v}^\dagger$ and $\hat{Q}_\beta \equiv \hat{b}_\beta + \hat{b}_\beta^\dagger$ are coordinate operators for the molecular vibration and the thermal bath mode β. Equation (8) describes the standard electron transfer interaction between the molecule and the two metals. The coupling (9) induces thermal relaxation of the molecular vibration because of interaction with the external thermal harmonic bath.

For the light-scattering problem, the minimal model for the electromagnetic field is represented by a single pumping (incident) mode i and a set of final accepting modes $\{f\}$. The unperturbed Hamiltonian now becomes $\hat{H}_0 = \hat{H}_M + \sum_{K=\{L,R,B\}} \hat{H}_K + \hat{H}_{\rm rad}$, where

$$\hat{H}_{\rm rad} = \nu_i \hat{a}_i^\dagger \hat{a}_i + \sum_f \nu_f \hat{a}_f^\dagger \hat{a}_f. \tag{10}$$

Here, $\hat{a}_i^\dagger$ ($\hat{a}_i$) and $\hat{a}_f^\dagger$ ($\hat{a}_f$) are creation (annihilation) operators for photons in the initial (pumping) and final modes i and $\{f\}$, respectively. For the system-radiation field interaction $\hat{V}_{\rm rad}$, we follow Ref. 30 in assuming that the field affects relative energies of single electron states localized on the molecule and in the leads. Specifically, we assume that the field acts as a time-dependent gate potential, affecting oscillations of the molecular energy level relative to the electrodes. We write it in the form

$$\hat{V}_{\rm rad} = -(\vec{p}_{\rm CT} \cdot \hat{\vec{E}})\hat{n} \tag{11}$$

[note that either $\hat{n}$ or $(\hat{n} - \bar{n})$ can be used in these expressions since only the time-dependent part of n contributes to the light-scattering processes], where $\hat{\vec{E}}$ is the electric field operator and $\vec{p}_{\rm CT}(\hat{n} - \bar{n})$ is the dipole associated with the charge transfer into/out of the molecule. The form (11) is valid when the molecular charging dynamics [determined by the rates Γ_L, Γ_R (defined in Eq. (33)] are slow relative to the metal dielectric relaxation measured by the plasma frequency. In Ref. 30, which considers a molecule adsorbed on a single metal substrate, this charge transfer dipole is represented by $\vec{p}_{\rm CT} = e\vec{d}$, where $\vec{d}$ is the distance vector from the electrode surface (or image plane) to the molecule and e is the electron charge. Again, such a model is valid at low frequencies, in which case electric field is perpendicular to the metal surface so that Eq. (11) becomes $\hat{V}_{\rm rad} = -ed\hat{E}\hat{n}$. In the present case, the determination of the charge transfer dipole, i.e., the dipole induced in the junction in response to molecular charging is a complex problem even in the electrostatic limit and depends on details of the junction geometry. In the simplest case of a point molecule located at midpoint between two metal planes, this dipole vanishes. A realistic junction does not usually possess this perfect symmetry, and charge transfer to/from the metal will usually lead to induced dipole. At the same time, for a molecule located between plasmon-sustaining metal structures, $p_{\rm CT}$ may be strongly enhanced if ν_i is close to the plasmon resonance frequency. Another source of coupling may be dominant in the case where the molecular permanent dipole $\vec{p}_M(n)$ depends strongly on its electronic population n [within our model, this implies that the molecular HOMO (highest occupied molecular orbital) and LUMO (lowest unoccupied molecular orbital) are associated with different molecular permanent dipoles]. In this case, $(d\vec{p}_M/dn)_{\bar{n}}$ provides another important contribution to $\vec{p}_{\rm CT}$.[33] In what follows, we carry the calculations assuming that $\vec{p}_{\rm CT}$ is known or has been determined.

In the following sections, we evaluate the Raman light scattering associated with this model. In a quasiclassical approach (Sec. III), the incident field is treated classically and the scattered radiation is evaluated from the resulting oscillating dipole. In a fully quantum treatment (Sec. IV), the field is an operator expressed in terms of its photon degrees of freedom. Equation (11) then takes the form

$$\hat{V}_{\rm rad} = -i\left(U_i(\hat{a}_i - \hat{a}_i^\dagger) + \sum_f U_f(\hat{a}_f - \hat{a}_f^\dagger)\right)\hat{n} \tag{12}$$

with

$$U_i = -\vec{p}_{\rm CT}\mathbf{K}_i\vec{E}_i, \tag{13a}$$
$$U_f = -\vec{p}_{\rm CT}\mathbf{K}_f\vec{\sigma}_f, \tag{13b}$$

where $\vec{E}_i$ is the electric field vector associated with the incident laser field, $\vec{\sigma}_f$ is the polarization vector (unit vector in the electrical field direction) associated with the outgoing mode f, and $\mathbf{K}_i$ and $\mathbf{K}_f$ are local tensors that depend on the corresponding incoming and outgoing frequencies, relating the incident and outgoing vector field to the corresponding local fields at the molecule. In particular, elements of these tensors contain all the information pertaining to possible local field enhancement associated with the given junction geometry. As stated above, in this paper we assume that these tensors are known, having been evaluated in a separate calculation (see, e.g., Ref. 15). In using the form (13a) for the incident field, we have expressed its amplitude explicitly, allowing for the formalism presented below to consider a steady state driven by an incoming photon mode populated by one photon.

III. RAMAN SCATTERING: THE QUASICLASSICAL APPROACH

Classically, light scattering is expressed as the radiation emitted by the dipole induced in the system by the driving fields, and its Raman component is obtained from the expansion of this induced dipole in the vibrational coordinate(s).[34] The latter are treated as classical motions within the Born-Oppenheimer approximation, so that the molecular level energy, driven by the external (classical) optical field $E_i(t) = E_i\cos(\nu_i t)$, is

$$\begin{aligned}\varepsilon_0(Q_v,t) &= \varepsilon_0(Q_v) + U_i\cos(\nu_i t)\\ &= \varepsilon_0(Q_v) + \frac{U_i}{2}(e^{i\nu_i t} + e^{-i\nu_i t}),\end{aligned} \tag{14}$$

where $U_i = \vec{p}_{\rm CT}\cdot\vec{E}_{\rm loc}$, with $\vec{E}_{\rm loc}$ being the local electric field associated with the incoming radiation. Furthermore, in the following we will assume that the vibrational deviation from equilibrium is small enough to allow the lowest-order expansion $\varepsilon_0(Q_v) = \varepsilon_0 + M_v Q_v$. The harmonic driving (14) of the level energy relative to the Fermi energy of the contacts yields an oscillating level occupation given by[35]

$$n(Q_v,t) = \sum_{k_1,k_2=-\infty}^{\infty} J_{k_1}\left(\frac{U_i}{\nu_i}\right)J_{k_2}\left(\frac{U_i}{\nu_i}\right)\int_{-\infty}^{\infty}\frac{dE}{2\pi}\frac{e^{i\nu_i(k_1-k_2)t}\sum_{K=\{L,R\}}\Gamma_K f_K(E)}{\left[E-\varepsilon_0(Q_v)-\nu_i k_1+\frac{i}{2}\Gamma\right]\left[E-\varepsilon_0(Q_v)-\nu_i k_2-\frac{i}{2}\Gamma\right]}, \tag{15}$$

where $J_k(x)$ is the Bessel function of the first kind. In (15), $\Gamma_K = 2\pi|V_K|^2\rho_K$ $[K = L,R;\ |V_K|^2 = \langle|V_k|^2\rangle_{k\in K} \equiv \int d\varepsilon_k|V(\varepsilon_k)|^2\rho_K(\varepsilon_k)]$ is the electron escape rate from the occupied molecular level into the lead K and $f_K(E)$ is the Fermi-Dirac distribution. The oscillating component of the level occupation is obtained from Eq. (15) to linear order in U_i in the form

$$n^{(1)}(Q_v,t) = \frac{U_i}{\nu_i}\sum_{K=\{L,R\}}\int_{-\infty}^{\infty}\frac{dE}{2\pi}{\rm Re}\left[\frac{\Gamma_K f_K(E)}{E-\varepsilon_0(Q_v)-i\Gamma/2}\left(\frac{e^{i\nu_i t}}{\left[E-\varepsilon_0(Q_v)-\nu_i+\frac{i}{2}\Gamma\right]}-\frac{e^{-i\nu_i t}}{\left[E-\varepsilon_0(Q_v)+\nu_i+\frac{i}{2}\Gamma\right]}\right)\right], \tag{16}$$

where we have used $J_k(x)\sim(x/2)^k/k!$ and $J_{-k}(x) = (-1)^k J_k(x)$. In our model, the corresponding oscillating dipole $\vec{p}$, hence the corresponding polarizability tensor $\alpha = \partial\vec{p}/\partial\vec{E}_i$, is proportional to this average level population, e.g., $\vec{p}(t) = \vec{p}_{\rm CT}n(t)$. For simplicity, we will henceforth also assume that $\vec{p}$ and $\vec{E}_i$ are parallel to each other and perpendicular to the substrate surface, and denote by α the corresponding nonzero component of the polarizability tensor.

In terms of $p_{\rm CT}$ we then have (to linear order in the external field)

$$p(Q_v,t) = E_i\left[\alpha(Q_v,\nu_i)e^{i\nu_i t} + \alpha^*(Q_v,\nu_i)e^{-i\nu_i t}\right], \tag{17}$$

where the polarizability is

$$\alpha(Q_v,\nu_i) = \frac{p_{\rm CT}^2}{2\nu_i}\sum_K\int_{-\infty}^{+\infty}\frac{dE}{2\pi}\Gamma_K f_K(E)\left(\frac{1}{[E-\varepsilon_0-i\Gamma/2][E-\varepsilon_0-\nu_i+i\Gamma/2]}-\frac{1}{[E-\varepsilon_0+i\Gamma/2][E-\varepsilon_0+\nu_i-i\Gamma/2]}\right). \tag{18}$$

The Raman polarizability is obtained by considering the term linear in Q_v. In the classical limit, the Stokes and anti-Stokes contributions are equal. We obtain

$$p_{\rm Raman}(t) = E_i\left(\alpha_v(\nu_i)e^{i(\nu_i\pm\omega_v)t} + \alpha_v^*(\nu_i)e^{-i(\nu_i\pm\omega_v)t}\right), \tag{19}$$

where

$$\begin{aligned}\alpha_v(\nu_i) = \left(\frac{\partial\alpha(Q_v,\nu_i)}{\partial Q_v}\right)_{Q_v=0} &= \frac{p_{\rm CT}^2 M_v}{4\pi\nu_i(\Gamma+i\nu_i)}\sum_{K=\{L,R\}}\Gamma_K\left[\frac{2\Gamma\nu_i(\varepsilon_0-\mu_K)}{[(\varepsilon_0+\nu_i-\mu_K)^2+(\Gamma/2)^2][(\varepsilon_0-\nu_i-\mu_K)^2+(\Gamma/2)^2]}\right.\\ &\left.+i\left(\frac{\varepsilon_0+\nu_i-\mu_K}{[(\varepsilon_0+\nu_i-\mu_K)^2+(\Gamma/2)^2]}+\frac{\varepsilon_0-\nu_i-\mu_K}{[(\varepsilon_0-\nu_i-\mu_K)^2+(\Gamma/2)^2]}-\frac{2(\varepsilon_0-\mu_K)}{[(\varepsilon_0-\mu_K)^2+(\Gamma/2)^2]}\right)\right],\end{aligned} \tag{20}$$

where we have taken $T \to 0$ to perform energy integration analytically.

From Eq. (19), the total scattered power is[36]

$$P = \frac{(\nu_i \pm \omega_v)^4}{3c^3} |\alpha_v(\nu_i) E_i|^2 . \tag{21}$$

(Note that the semiclassical approach assumes $\nu_i \gg \omega_v$ and the Raman polarizability is obtained in terms of ν_i only.) Equations (20) and (21) constitute our main classical limit results, expressing the charge transfer contribution to the Raman scattering, here derived for the response of the molecular bridge in a (generally biased) molecular conduction junction. The bias potential enters explicitly through the chemical potentials μ_K $(K = L, R)$ in Eq. (20).

To facilitate comparison with the results of Ref. 30, it is convenient to consider the scattering function $A(\nu_i, \nu_i \pm \omega_v)$ defined in Eq. (14) of that paper.[37] In the quasiclassical case, this function depends only on ν_i and we denote it by $A_{sc}(\nu_i)$. A relationship between this function and the Raman polarizabilty may be found by comparing Eqs. (13) and (18) of Ref. 30, and recalling that in Ref. 30, case $ed = p_{\rm CT}$. This leads to

$$A_{sc}(\nu_i) = \frac{\alpha_v(\nu_i)}{2p_{\rm CT}^2 M_v}. \tag{22}$$

A comparison of the scattering function A calculated using (22) and (20), our quantum results from Sec. IV and the results of Ref. 30, is provided in Sec. V.

Note that in evaluating Eqs. (20) and (22), we have assumed that all the dependence on Q_v comes from its effect on the molecular electronic energy. Other contributions could come from the possible dependence of the junction transport properties (e.g., the rate parameters Γ) on Q_v through the molecule-metal distance, or from the dependence on Q_v of the metal electronic response.[38]

IV. QUANTUM CONSIDERATION

As a quantum problem, Raman scattering in the present model can be evaluated by following the approach of our previous publications[20,21] modified to take into account the different system-radiation field coupling. First, we consider the photon flux from the molecule to an empty accepting mode f. We start from Eq. (25) of Ref. 21:

$$J_{M\to f} = -\int_{-\infty}^{+\infty} d(t-t')\, \Pi_f^{>}(t'-t) \mathcal{G}^{<}(t-t'), \tag{23a}$$

where $\Pi_f^{>}(t'-t)$ is the molecular self-energy due to coupling to the mode f, given, for a free unoccupied mode, by

$$\Pi_f^{>}(t'-t) = -i|U_f|^2 e^{-i\nu_f(t'-t)}. \tag{23b}$$

This leads to

$$J_{M\to f} = i|U_f|^2 \mathcal{G}^{<}(\nu_f). \tag{24}$$

In Eqs. (23a) and (24), $\mathcal{G}^{<}(t-t')$, the Fourier transform of which is $\mathcal{G}^{<}(\nu_f)$, is the lesser projection of the two-particle Green's function $\mathcal{G}$ defined by the form (11) of the molecular coupling to the electromagnetic field, i.e., a density-density correlation function given on the Keldysh contour by

$$\mathcal{G}(\tau_1, \tau_2) \equiv -i\langle T_c\, \hat{n}(\tau_1)\, \hat{n}(\tau_2)\rangle, \tag{25}$$

where $\tau_{1,2}$ are variables on the Keldysh contour and T_c is the contour ordering operator. The time evolution in (25) is defined by the Hamiltonians (1)–(11) and the average is over an electronic steady state of the biased junction in which the interaction with the accepting modes $\{f\}$ is absent. Note that Eq. (24) is of second order in the interaction with the outgoing modes, so that to this order the Green's function (25) can be evaluated while disregarding this interaction.

Next, regarding the interactions between the molecular electronic state and the incoming radiation field U_i, as well as with the molecular vibration M_v, as perturbations, we derive (see Appendix A) a perturbative expression for the Green's function (25) within the lowest relevant order (second) in each of these interactions. The resulting expression in which the time evolutions are defined in terms of the quadratic Hamiltonian (2) may be expanded using Wicks theorem and expressed as a diagrammatic expansion. As discussed in Appendix A, we focus only on those diagrams that are relevant for the Raman process under discussion. The results of Ref. 30 provide useful guidelines for identifying these diagrams, which are displayed in Fig. 1. By substituting the corresponding expressions (A2), for the Green's function (25) into (24), we obtain the outgoing Raman flux into an accepting mode f that results from pumping the molecule by mode i:

$$\begin{aligned} J_{i\to f} = |U_i|^2|U_f|^2|M_v|^2 \int_{-\infty}^{+\infty} d(t-t') e^{i\nu_f(t-t')} \\ \times \int_c d\tau_1 \int_c d\tau_2 \int_c d\tau_3 \int_c d\tau_4 \tilde{D}_i(\tau_1,\tau_2) D_v(\tau_3,\tau_4) \\ \times [G(t',\tau_4)G(\tau_4,\tau_2)G(\tau_2,t')\, G(t,\tau_1)G(\tau_1,\tau_3)G(\tau_3,t) \end{aligned} \tag{26a}$$

$$+ G(t',\tau_2)G(\tau_2,\tau_4)G(\tau_4,t')\, G(t,\tau_3)G(\tau_3,\tau_1)G(\tau_1,t) \tag{26b}$$

$$+ G(t',\tau_2)G(\tau_2,\tau_4)G(\tau_4,t')\, G(t,\tau_1)G(\tau_1,\tau_3)G(\tau_3,t) \tag{26c}$$

$$+ G(t',\tau_4)G(\tau_4,\tau_2)G(\tau_2,t')\, G(t,\tau_3)G(\tau_3,\tau_1)G(\tau_1,t)]. \tag{26d}$$

Equation (26) is the main quantum result of this paper. The terms (a)–(d) in this equation correspond to the similarly labeled diagrams in Fig. 1. In Eq. (26), $\tilde{D}_i$ is *the momentum* Green's function of the pumping mode i:

$$\tilde{D}_i(\tau_1,\tau_2) = -i\langle T_c \hat{P}(\tau_1)\hat{P}(\tau_2)\rangle, \tag{27}$$

where $\hat{P}_i \equiv -i(\hat{a}_i - \hat{a}_i^\dagger)$, D_v is *the coordinate* Green's function of molecular vibration v,

$$D_v(\tau_3,\tau_4) = -i\langle T_c \hat{Q}_v(\tau)\hat{Q}_v(\tau')\rangle, \tag{28}$$

where $\hat{Q}_v \equiv \hat{v} + \hat{v}^\dagger$, and G is *the single-particle* electron Green's function.

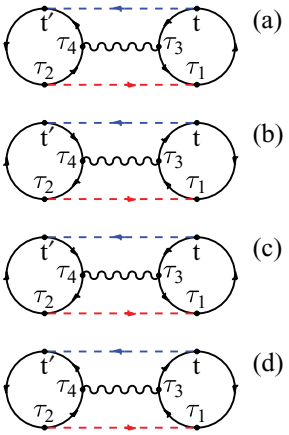

FIG. 1. (Color online) Diagrams relevant for the charge transfer contribution to SERS. Dashed lines represent Green's functions of the free photon modes (pumping and accepting), wavy lines represent Green's functions of molecular vibration, directed solid lines indicate electronic single-particle Green's functions with arrows indicating electron propagation. Time labels correspond to the integration variables in Eq. (26). The four diagrams represent scattering events of particles and holes, interacting via electromagnetic field and molecular vibration.

$$G(\tau,\tau') = -i\langle T_c\, \hat{d}(\tau)\, \hat{d}^{\dagger}(\tau')\rangle. \tag{29}$$

Note that the contour variables τ_1, τ_2, τ_3, τ_4 in Eq. (26) are yet to be projected. From all possible projections, we are interested only in the rates, i.e., τ_1 and τ_2 as well as τ_3 and τ_4 have to be on opposite branches of the Keldysh contour.[39] These projections involve the projected Green's functions G, $\tilde{D}_i$, and D_v, which enter Eq. (26) and take the following forms in the lowest-order approximation employed here:

(a) In the spirit of the perturbation expansion employed above, the Green's function $\tilde{D}_i$ for the pumping mode can be taken for a free incoming photon, namely,[40]

$$\tilde{D}_i^{>,<}(t_1 - t_2) = -ie^{\pm i\nu_i(t_1-t_2)}. \tag{30}$$

(b) Similarly, on the simplest level of description, the vibrational mode Green's function D_v of the molecular vibration can be taken as the noninteracting phonon Green's function, the lesser and greater projections of which are (in energy space)[41]

$$D_v^{(0)>}(\omega) = -2\pi i[N_v\delta(\omega+\omega_v) + [N_v+1]\delta(\omega-\omega_v)], \tag{31a}$$

$$D_v^{(0)<}(\omega) = -2\pi i[N_v\delta(\omega-\omega_v) + [N_v+1]\delta(\omega+\omega_v)], \tag{31b}$$

where $N_v = N_{\rm BE}(\omega_v)$ is the thermal Bose-Einstein population of the molecular vibration.

(c) Finally, on the same level of description, the single-electron Green's function G can be replaced by $G^{(0)}$, the electronic Green's function of the resonant electronic level model (disregarding electron-phonon coupling). The lesser and greater projections of this function are (in energy space)[41]

$$G^{(0)>}(E) = -i\frac{\sum_{K=L,R}\Gamma_K(E)[1-f_K(E)]}{(E-\varepsilon_0)^2 + [\Gamma(E)/2]^2}, \tag{32a}$$

$$G^{(0)<}(E) = i\frac{\sum_{K=L,R}\Gamma_K(E) f_K(E)}{(E-\varepsilon_0)^2 + [\Gamma(E)/2]^2}. \tag{32b}$$

In Eqs. (32), $f_K(E)$ is the Fermi-Dirac distribution,

$$\Gamma_K(E) = 2\pi\sum_{k\in K}|V_k|^2\delta(E-\varepsilon_k) \tag{33}$$

is the electron escape rate to contact K ($K = L,R$), and $\Gamma(E) = \Gamma_L(E) + \Gamma_R(E)$. In the wide-band approximation employed below, Γ_K is taken to be energy independent.

This lowest-order approximation is the same as that employed in Ref. 30. Indeed, as discussed below, the above choice of Green's functions $\tilde{D}_i$, D_v, and G together with the equilibrium condition ($\mu_L = \mu_R$) and zero-temperature assumption, reproduces the results of Ref. 30.

Details of the calculation in which Eq. (26) is projected onto real-time axes using Eqs. (30)–(33) are presented in Appendix B. To facilitate comparison with the zero-temperature equilibrium result of Ref. 30, we note that in that paper the scattering flux equivalent to (26) is obtained in the form [cf. Eqs. (11)–(15) of Ref. 30]

$$J_{i\to f} = 2\pi|H'|^2\delta(E_i - E_f) \tag{34}$$

with[42]

$$H' = M_v E^2 p_{\rm CT}^2 A(\nu_i,\nu_f), \tag{35}$$

where the scattering amplitude $A(\nu_i,\nu_f)$ (Ref. 37) is given as a sum $A = \sum_{i=1}^{6} A_i$ of different contributions associated with different orderings by which the different interactions $\hat{V}_M$ and $\hat{V}_{\rm rad}$, Eqs. (7) and (11), enter in the perturbative calculation and also with the different electronic processes (electron or hole exchange between molecule and substrate) involved (see Ref. 30 and Appendix B for details). Note that in Ref. 30 no distinction is made between the incident and the local field, therefore, in comparing results, the tensors $\mathbf{K}$ in Eqs. (13) should be set to unities. With this provision, we show in Appendix B that Eq. (13) yields the Stokes scattering flux in the form (34), (35) where A is given by

$$A = \sum_{i=1}^{6} A_i, \tag{36}$$

where

$$A_1 \equiv A(-\omega_v,\nu_f), \tag{37a}$$
$$A_2 \equiv A(-\omega_v,-\nu_i), \tag{37b}$$
$$A_3 \equiv A(\nu_i,\omega_v), \tag{37c}$$
$$A_4 \equiv A(-\nu_f,\omega_v), \tag{37d}$$
$$A_5 \equiv A(\nu_i,\nu_f), \tag{37e}$$
$$A_6 \equiv A(-\nu_f,-\nu_i), \tag{37f}$$

and

$$A(x,y) = i\int_{-\infty}^{+\infty}\frac{dE_1}{2\pi}\int_{-\infty}^{+\infty}\frac{dE_2}{2\pi}\int_{-\infty}^{+\infty}\frac{dE_3}{2\pi} \times\left[G^{(0)<}(E_1)\frac{G^{(0)>}(E_2)}{E_2-E_1+x-i\delta}\frac{G^{(0)>}(E_3)}{E_3-E_1+y-i\delta} + G^{(0)>}(E_1)\frac{G^{(0)<}(E_2)}{E_1-E_2+x-i\delta}\frac{G^{(0)<}(E_3)}{E_1-E_3+y-i\delta}\right], \quad (38)$$

which provide the generalization to nonequilibrium (biased junction) and finite temperature of the result of Ref. 30. It is easily seen to give the latter results in the zero-temperature equilibrium limit.

We conclude this section by noting that this calculation could be carried on a more advanced level by taking into account the mutual influence of vibrational and electronic degrees of freedom in the current-carrying junction. This is often described in the self-consistent Born approximation (SCBA),[41] where these mutual effects are accounted for by including, in the self-energy Π of the molecular vibrational mode, the contribution due to coupling to the tunneling electron

$$\Pi^{el}(\tau,\tau') \equiv -i|M_v|^2 G(\tau,\tau')G(\tau',\tau) \quad (39)$$

and in the electron self-energy Σ, a term due to coupling to this mode

$$\Sigma^{ph}(\tau,\tau') \equiv i|M_v|^2 D_v(\tau,\tau')G(\tau,\tau'), \quad (40)$$

and evaluating the vibrational and electronic Green's functions D_v and G, respectively, as self-consistent solutions of the coupled Dyson equations

$$D_v(\tau,\tau') = D_v^{(0)}(\tau,\tau') + \int_c d\tau_1\int_c d\tau_2\, D_v^{(0)}(\tau,\tau_1) \times[\Pi^{ph}(\tau_1,\tau_2)+\Pi^{el}(\tau_1,\tau_2)]D_v(\tau_2,\tau'), \quad (41)$$

$$G(\tau,\tau') = G^{(0)}(\tau,\tau') + \int_c d\tau_1\int_c d\tau_2\, G^{(0)}(\tau,\tau_1) \times\Sigma^{ph}(\tau_1,\tau_2)\,G(\tau_2,\tau'). \quad (42)$$

(Note that our choice of $G^{(0)}$, taken to include the molecule-lead coupling, leaves Σ^{ph} as the only contribution to the self-energy.) The lesser and greater projections of the Green's functions $D_v^{(0)}$ and $G^{(0)}$ are given by Eqs. (31) and (32). Π^{ph} is the phonon self-energy due to coupling to the thermal boson bath

$$\Pi^{ph}(\tau,\tau') \equiv \sum_\beta |W_\beta|^2 D_\beta(\tau,\tau'), \quad (43)$$

where $D_\beta(\tau,\tau') = -i\langle T_c\,\hat{Q}_\beta(\tau)\,\hat{Q}_\beta(\tau')\rangle_0$ is the *coordinate* free phonon Green's function for mode β of this bath. Π^{ph} is associated with the vibrational relaxation rate

$$\gamma(\omega) \equiv -2\,\mathrm{Im}\Pi^r(|\omega|) = \sum_\beta |W_\beta|^2\delta(\omega-\omega_\beta), \quad (44)$$

which, in a wide-band approximation similar to that taken above for the electronic escape rate, may be taken constant when $\omega_v \gg \gamma(\omega_v)$. For details of the SCBA implementation, see, e.g., Ref. 43.

V. RESULTS AND DISCUSSION

In this section, we present numerical calculations of the charge transfer contribution to the Raman signal, based on the quantum results [Eqs. (34)–(38)] and the quasiclassical calculation [Eqs. (20) and (22)]. Unless otherwise stated, the parameters used in these calculations are $T = 300$ K, $\Gamma_L = \Gamma_R = 0.25$ eV, $\omega_v = 0.2$ eV, $M = 0.1$ eV, and $\gamma = 10^{-4}$ eV. The bias was applied symmetrically, i.e., $\mu_{L,R} = E_F \pm |e|V_{sd}/2$, and the Fermi energy was chosen as the energy origin $E_F = 0$. The frequency of incoming photon is taken $\nu_i = 2$ eV and the outgoing frequency is taken to represent the Stokes peak $\nu_f = \nu_i - \omega_v = 1.8$ eV. Under our control is the bias voltage V_{sd} itself, and in principle also the gate potential that determines the position ε_0 of the molecular level relative to the Fermi energy. All calculations were performed on an energy grid of step 10^{-3} eV, spanning the region from -10 to 10 eV.

Figure 2 shows the Stokes scattering amplitude $|A(\nu_i,\nu_f = \nu_i-\omega_v)|$ calculated from Eqs. (34)–(38) in the quantum case and from Eqs. (20) and (22) in the quasiclassical approximation for an equilibrium system $V_{sd} = 0$. The results can be compared to those presented in Fig. 2 of Ref. 30 (note, however, that our calculations are done at $T = 300$ K). It shows the absolute value of the total Stokes scattering amplitude versus position ε_0 of the molecular level relative to the Fermi energy, obtained from the quasiclassical approximation [Eqs. (20) and (22)] and the quantum approach [Eqs. (34)–(38)]. The following points should be noted: (a) Good agreement with

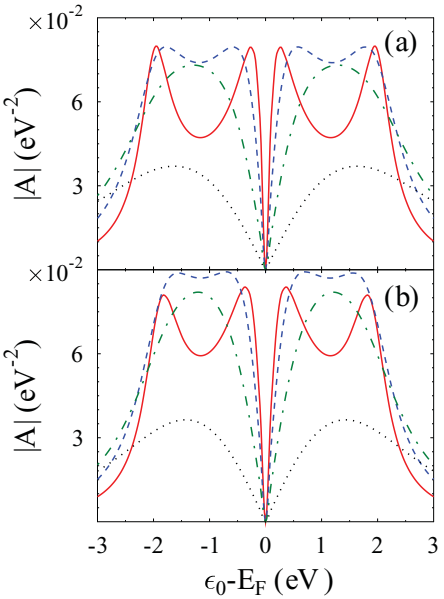

FIG. 2. (Color online) Absolute value of the total Stokes scattering amplitude vs gate voltage calculated at $V_{sd} = 0$ within (a) the quasiclassical approach [Eqs. (20) and (22)] and (b) the quantum calculation [Eqs. (34)–(38)]. Shown are results for $\Gamma_{L,R} = 0.25$ (solid line, red), 0.5 (dashed line, blue), 1.0 (dashed-dotted line, green), and 2.0 eV (dotted line, black). See text for other parameters.

the result of Ref. 30 is obtained in this equilibrium case. (b) The symmetric character of the curve about $\varepsilon_0 = E_F$ is due to the particle-hole symmetry of our model, i.e., particle transport contribution to scattering amplitude [first term in Eq.(38)], and is equivalent to the hole transport contribution [second term in Eq.(38)] for a molecular level positioned symmetrically above and below Fermi energy, respectively. (c) Destructive interference between the electron and hole scattering processes leads to suppression of Raman signal at $\varepsilon_0 = E_F$. (d) The signal also drops when $|\varepsilon_0 - E_F|$ exceeds the incident frequency ν_i since electron transfer between metal and molecule can not be affected (and consequently no molecule-contact dipole excitation can be created) in this far-off-resonant regime. (e) The quasiclassical calculation provides an excellent approximation to the quantum result in this case.

Figure 3 demonstrates the generalization of the previous results to the nonequilibrium (biased) junction. Shown is absolute value of the total Stokes scattering amplitude $|A|$ versus the applied bias, calculated for $\varepsilon_0 = 1.8$ V within the quasiclassical and the quantum schemes. Consider first the results of the quantum calculation. Similar to the equilibrium case, the Stokes scattering amplitude has a nonmonotonic dependence on the energy difference between the molecular level and the leads chemical potential(s), which changes with the bias potential. Again, the signal drops at the far-off-resonance regime. In particular, for the $\Gamma_{L,R} = 0.25$ eV case (solid line, red), the peak at $V_{sd} = 0$ ($\varepsilon_0 - E_F = \nu_i - \omega_v$) corresponds to opening of a scattering channel, when an electron starting at $E_F - \omega_v$ is scattered by the molecule and ends just above the Fermi energy. A second peak is

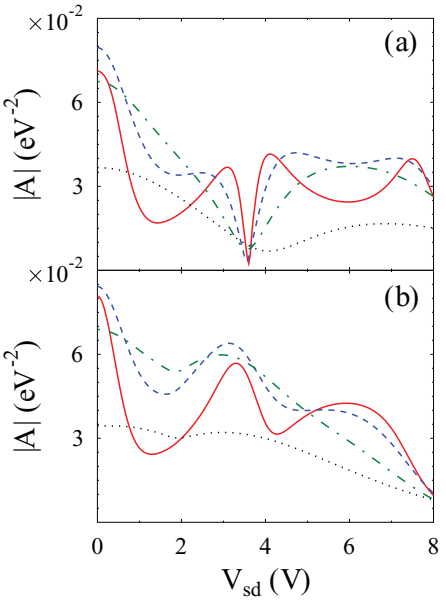

FIG. 3. (Color online) Absolute value of the total Stokes scattering amplitude [Eqs. (36)–(38)] vs bias calculated at $\varepsilon_0 - E_F = 1.8$ V within (a) the quasiclassical approach [Eqs. (20) and (22)] and (b) the quantum calculation [Eqs. (34)–(38)]. Shown are results for $\Gamma_{L,R} = 0.25$ (solid line, red), 0.5 (dashed line, blue), 1 (dashed-dotted line, green), and 2 eV (dotted line, black). Other parameters are as in Fig. 2.

at $V_{sd} = 3.2$ V ($\varepsilon_0 - \mu_L = \omega_v$). Here, a metal electron of energy near μ_L is scattered by the molecule and ends near the molecular level. We could not identify a simple origin for the third peak. We note in passing that at equilibrium (e.g., for a molecule adsorbed on a single metal substrate) the dependence of the Raman signal on the electrode potential (which, for the equilibrium case, can be expressed by ε_0) has been an indicator for the electron-transfer ("chemical") contribution to the Raman enhancement. The dependence on bias potential seen here can serve a similar purpose.

Turning now to the quasiclassical calculation, it again agrees with the quantum result provided that the molecular level is outside the window between the Fermi energies of the two contacts ($V_{sd} < 3.6$ V for $\varepsilon_0 = 1.8$ eV). Above this threshold, marked deviations are seen. The reason for this difference is that the quasiclassical calculation disregards the blocking of scattering channels by electron exclusion when molecular level(s) start to be populated. Indeed, the quasiclassical approach is essentially a scattering-based theory, and the inadequacy of scattering theory in describing inelastic effects in nonequilibrium electronic transport junctions is a familiar observation.[44,45]

Figure 4 shows the dependence of the total Stokes scattering amplitude calculated from Eqs. (34)–(38), on both the frequency of the pumping mode and the bias potential. The calculation is done for $\varepsilon_0 = 1.8$ eV and $\Gamma_{L,R} = 0.25$ eV within the model assumptions [Eqs. (31) and (32)]. The structure in the bias dependence of the Stokes amplitude for fixed ν_i was discussed above. For $V_{sd} = 0$, the amplitude as a function of ν_i naturally peaks around the molecular level position, indicating the opening of a channel for electron scattering that starts at E_F. This behavior was demonstrated also in Fig. 3 of Ref. 30. Deviation from this peak structure at higher bias sets in when the lead chemical potential comes into resonance with the molecular level (at $V_{sd} = 3.6$ V), opening the channel for electron scattering that is responsible for the second peak in Fig. 3. Viewed with respect to the incoming frequency ν_i, contributions from the initial, intermediate, and final states for electron scattering are most pronounced in the region of maximum local molecular density of states, that is, close to ε_0, which is reflected in the scattering amplitude (hence the scattering flux) dependence on the bias voltage (for a more

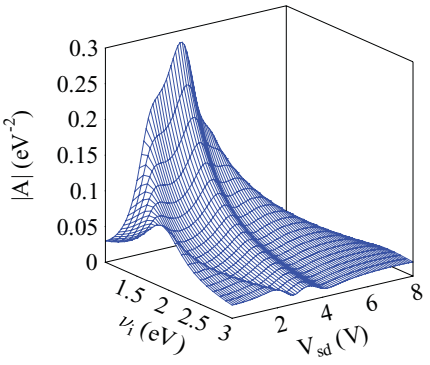

FIG. 4. (Color online) Absolute value of the total Stokes scattering amplitude [Eqs. (34)–(38)] vs bias V_{sd} and the incoming frequency ν_i calculated for $\varepsilon_0 - E_F = 1.8$ eV. See text for other parameters.

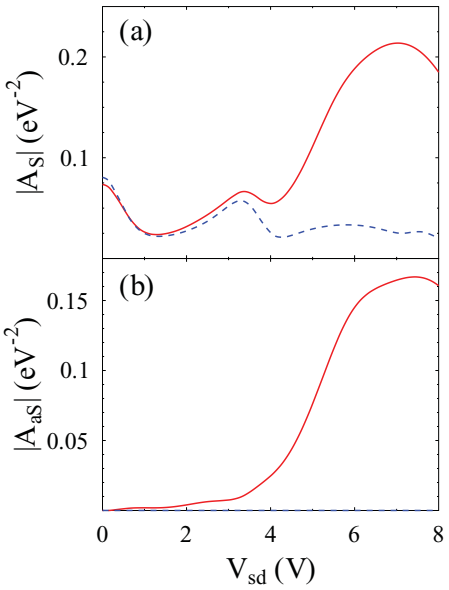

FIG. 5. (Color online) Absolute value of the total (a) Stokes and (b) anti-Stokes amplitudes, plotted against the bias voltage V_{sd} for a molecular level near $\varepsilon_0 - E_F = 1.8$ V. Shown are noninteracting (dashed line, blue) and SCBA (solid line, red) results. See text for other parameters.

detailed discussion of this line-shape structure, see Refs. 46 and 47).

The calculations presented above are based on the lowest-order approximation [Eqs. (31) and (32)]. In this level of approximation, the electron-vibration coupling, which is responsible for the Raman shift, is disregarded in the expressions for single-particle Green's functions. Figure 5 shows results obtained when the electron-vibration interaction is treated within the self-consistent Born approximation [Eqs. (39)–(42)]. For simplicity, we treat the vibrational degree of freedom in the quasiparticle approximation,[40] whereupon hybridization of the molecular vibration with states of the boson bath is disregarded, while the average vibrational population is influenced by the electronic flux. In turn, the electron Green's function is affected by the heated vibration. For details of the SCBA implementation in the quasiparticle approximation, see, e.g., Ref. 48. Figure 5 shows the absolute values of Stokes and anti-Stokes scattering amplitudes as functions of bias. The lowest-order result (dashed line) is compared to the SCBA (solid line). We see that for our (reasonable) choice of molecular and junction parameters, incorporating electron-vibration interaction does not make an essential difference in the Stokes signal below the threshold for resonance transmission (here, $V_{sd} = 3.6$ V). The reason for this is that heating of the molecular vibration in this regime is inefficient. Above this threshold, however, the Stokes signal calculated within the SCBA is markedly different from the low-order result. The influence of this correction on anti-Stokes scattering is even more pronounced. The latter is proportional to the average vibrational mode population, and even inefficient heating makes an important contribution to this signal.

VI. CONCLUSION

We have presented a model for the charge transfer contribution to SERS in a molecular junction. This model is a nonequilibrium finite-temperature generalization of an approach describing SERS for a molecule chemisorbed on metal surface.[30] Physically, this contribution to light scattering stems from the oscillating dipole induced in the system by charge transfer from the metal(s). In addition to the mechanism considered in Ref. 30, whereupon this dipole reflects the time-dependent polarization at the metal-molecule interface, we have identified another potential origin for this scattering mechanism: the dependence of the molecular permanent dipole on its charging state. We have presented a quasiclassical treatment of this problem as well as a fully quantum NEGF approach. Both reproduce the results of Ref. 30 when used in the appropriate limit: zero-temperature equilibrium situation, treated at the lowest order in the molecular electronic-vibrational interaction. The quasiclassical approach was shown to provide a reliable approximation for the full quantum result within its expected range of validity: in the weak junction-radiation field coupling considered here, and the far-off-resonance tunneling case where the molecular level occupation is not affected by its coupling to the leads. We have also used the self-consistent Born approximation to account for the electron-vibration interaction on the molecule, and found the effect of this correction to be small in the low bias regime, while becoming dominant for the anti-Stokes component of the scattered radiation above the resonance conduction threshold.

Our results provide a framework for describing the charge transfer ("chemical") contribution to Raman scattering from a molecular junction. They supplement our previous studies[20,21,49,50] that focus on the effect of the biased junction environment on Raman scattering that originates in the molecule itself. Two points regarding both mechanisms are noteworthy:

(a) Both mechanisms are affected, in different ways, by charge transfer between the metal substrate and the molecule; however, in the process that originates in the molecule, charge transfer from the metal substrate(s), in particular in biased and/or gated junctions, modifies a molecular process that exists also away from the metal. In contrast, for the so-called chemical mechanism, charge transfer is essential: the corresponding contribution vanishes when it is disallowed. It is therefore important only in direct proximity to the metal surface. Since in molecular conduction junctions we naturally consider molecules in such close proximity, both mechanisms are potentially important.

(b) Both mechanisms reflect the properties of the local electromagnetic field and are therefore affected by the electromagnetic enhancement mechanism in the same way. The main difference between them arises from the additional enhancement that takes place when certain resonance conditions are obeyed. In standard molecular Raman scattering, resonance implies matching between the incident photon and the molecular excitation energy. In the charge transfer mechanism, the closest we come to resonance is when the incident photon bridges the gap between the vicinity of the substrate Fermi energy (where an electron-hole pair is created or destroyed in the Raman Stokes or anti-Stokes process) and

a relevant molecular level. Experimentally, this is reflected in the bias and gate potential dependence of such resonance condition. Note that in a biased junction, two such Fermi energies can contribute. This is the origin of the nonmonotonic behavior of the scattering signal with bias and gate potentials, and with the incident mode frequency, as discussed above.

Finally, we note that as a simple model for the behavior of a molecular junction under illumination, we have followed previous works that model this effect by assuming that the electromagnetic field affects oscillations in the molecular energy position relative to the metal(s) Fermi energy. Alternatively, this effect may be represented as an oscillating bias potential. Both models yield qualitatively similar results, and comparison between them will be presented elsewhere.

ACKNOWLEDGMENTS

We thank B. Fainberg for helpful discussions. A.N. acknowledges support by the Israel Science Foundation, the Israel-US Binational Science Foundation, the European Research Council under the European Union's Seventh Framework Program (FP7/2007-2013; ERC Grant No. 226628) and the Israel - Niedersachsen Research Fund. M.O. acknowledges support by the Israeli Ministry of Science and Technology, under the program for advancement of women in science and technology. M.G. gratefully acknowledges support by the DOE (Early Career Award, DE-SC0006422), the BSF (2008282), and the Hellmann Family Foundation.

APPENDIX A: PERTURBATIVE EVALUATION OF THE DENSITY-DENSITY CORRELATION FUNCTION

To evaluate the nonequilibrium charge transfer assisted Raman scattering from Eq. (24), we follow the lines of Ref. 21. Guided by the zero-temperature equilibrium calculation of Ref. 30, we focus on terms that correspond to three scattering events undergone by the tunneling electron: one each with the incoming and outgoing photons, and one with the molecular vibration. Such terms should contain each of the corresponding interactions at the second order of perturbation theory. Equation (24) is already of the second order in the coupling to the outgoing photon (through the corresponding self-energy), thus the two-particle Green's function (25) should be written to second order in both the coupling to the incoming photon and to the molecular vibration. The required expression is obtained in a standard way expanding the contour evolution operator in the interaction representation to fourth order in perturbation $\hat{V} = M(\hat{v} + \hat{v}^\dagger)\hat{n} - iU_i(\hat{a}_i - \hat{a}_i^\dagger)$:

$$\mathcal{G}(\tau,\tau') \approx \frac{(-i)^5}{4!}\int_c d\tau_1 \int_c d\tau_2 \int_c d\tau_3 \int_c d\tau_4 \times \langle T_c\, \hat{n}(\tau)\,\hat{n}(\tau')\,\hat{V}(\tau_1)\,\hat{V}(\tau_2)\,\hat{V}(\tau_3)\,\hat{V}(\tau_4)\rangle \quad \text{(A1)}$$

and keeping terms that are of the second order in each of the couplings M and U_i. Time evolution in (A1) is under Hamiltonian (1) without coupling to molecular vibration (7) and optical field (11).

The resulting expression is evaluated by employing Wick's theorem. This procedure produces a set of diagrams, which roughly can be separated into three groups: (i) renormalization of electron propagator(s) due to coupling to external fields, (ii) polarization of the environment due to presence of excess charge, and (iii) electron scattering due to interaction with photons and phonons. In terms of the Bethe-Salpeter equation[51] (two-particle propagator), the first category is characterized by diagrams where at least one of the fields interacts with only one of the particles. At our (low-order) level of description, the second category is characterized by a polarization bubble renormalized by the interaction with the external fields. Raman scattering is described by diagrams of the third category. These diagrams are presented in Fig. 1. They describe electron-hole [Figs. 1(a) and 1(b)] and electron-electron [Figs. 1(c) and 1(d)] scatterings (see the following). Their sum is given by

$$\begin{aligned}\mathcal{G}(\tau,\tau') &= -i|U_i|^2|M_v|^2 \\ &\times \int_c d\tau_1 \int_c d\tau_2 \int_c d\tau_3 \int_c d\tau_4 \tilde{D}_i(\tau_1,\tau_2) D_v(\tau_3,\tau_4) \\ &\times [G(t',\tau_4)G(\tau_4,\tau_2)G(\tau_2,t')\, G(t,\tau_1)G(\tau_1,\tau_3)G(\tau_3,t) \\ &+ G(t',\tau_2)G(\tau_2,\tau_4)G(\tau_4,t')\, G(t,\tau_3)G(\tau_3,\tau_1)G(\tau_1,t) \\ &+ G(t',\tau_2)G(\tau_2,\tau_4)G(\tau_4,t')\, G(t,\tau_1)G(\tau_1,\tau_3)G(\tau_3,t) \\ &+ G(t',\tau_4)G(\tau_4,\tau_2)G(\tau_2,t')\, G(t,\tau_3)G(\tau_3,\tau_1)G(\tau_1,t)]. \end{aligned} \quad \text{(A2)}$$

Substituting this into (24) leads to (26).

APPENDIX B: THE ZERO-TEMPERATURE EQUILIBRIUM CASE

Here, we outline the evaluation of the nonequilibrium Raman flux, Eq. (26), and show that the resulting expression reduces to the results of Ref. 30 in the equilibrium zero-temperature limit. In Ref. 30, the scattering flux equivalent to (IV) is given [cf. Eqs. (11)–(15) in that paper] in the form $J_{i\to f} = 2\pi|H'|^2\delta(E_i - E_f)$ where $H' = M_c E^2 p_{\rm CT}^2 A(\nu_i,\nu_f)$ and $A = \sum_{i=1}^6 A_i$. These contributions correspond to six *sequences* of occurrences of the following three events: (a) absorption from the pumping mode i, (b) emission into the accepting mode f, and (c) vibrational excitation resulting from the electron interaction with the molecular vibration v:

$$A_1 \equiv A(-\omega_v,\nu_f)(\hat{a}_f^\dagger \to \hat{a}_i \to \hat{v}^\dagger), \quad \text{(B1a)}$$

$$A_2 \equiv A(-\omega_v,-\nu_i)(\hat{a}_i \to \hat{a}_f^\dagger \to \hat{v}^\dagger), \quad \text{(B1b)}$$

$$A_3 \equiv A(\nu_i,\omega_v)(\hat{v}^\dagger \to \hat{a}_f^\dagger \to \hat{a}_i), \quad \text{(B1c)}$$

$$A_4 \equiv A(-\nu_f,\omega_v)(\hat{v}^\dagger \to \hat{a}_i \to \hat{a}_f^\dagger), \quad \text{(B1d)}$$

$$A_5 \equiv A(\nu_i,\nu_f)(\hat{a}_f^\dagger \to \hat{v}^\dagger \to \hat{a}_i), \quad \text{(B1e)}$$

$$A_6 \equiv A(-\nu_f,-\nu_i)(\hat{a}_i \to \hat{v}^\dagger \to \hat{a}_f^\dagger), \quad \text{(B1f)}$$

where the expressions in parentheses indicate the event sequence, for example, $\hat{a}_f^\dagger \to \hat{a}_i \to \hat{v}^\dagger$ shows creation of the final photon preceding the absorption of the initial photon with the creation of the vibrational quantum trailing both. Each of these amplitudes is a sum of two terms corresponding to

electron and hole electron transport [see Eq. (15) of Ref. 30]

$$A(x,y) \equiv \int_{-\infty}^{E_F} dE\rho_0(E) \int_{E_F}^{+\infty} dE' \frac{\rho_0(E')}{E'-E+x-i\delta} \times \int_{E_F}^{+\infty} dE'' \frac{\rho_0(E'')}{E''-E+y-i\delta} - \int_{E_F}^{+\infty} dE\rho_0(E) \int_{-\infty}^{E_F} dE' \frac{\rho_0(E')}{E-E'+x-i\delta} \times \int_{-\infty}^{E_F} dE'' \frac{\rho_0(E'')}{E-E''+y-i\delta}, \quad \text{(B2)}$$

where

$$\rho_0(E) = \frac{1}{2\pi} \frac{\Gamma}{(E-\varepsilon_0)^2 + (\Gamma/2)^2} \quad \text{(B3)}$$

is the local electron density of states and E_F is the Fermi energy of the metal substrate. For example, by using (B2) in (B1a), one gets scattering amplitude for a process with two intermediate states characterized by energies E'' and E' and incoming energy $\pm E$ for electron/hole. The first and second terms in Eq. (B2) correspond to electron and hole transport, respectively.

In our calculation, the evaluation of the Raman flux (26) leads to a sum of products. Contributions to the Raman scattering flux in our scheme result from two amplitudes $A^{t_1}_{s_1}$ and $A^{t_2}_{s_2}$ (bubble diagrams in Fig. 1). Here, $s_1,s_2 = \{1,2,3,4,5,6\}$ is one of *the sequences* of scattering events defined in Eq. (B1) and $t_{1,2} = \{1,2\}$ is one of the types (electron or hole) of transport. The corresponding contribution to the squared amplitude that enters into the Raman flux $T_{(s_2,t_2)\leftarrow(s_1,t_1)} \equiv [A^{t_2}_{s_2}]^* A^{t_1}_{s_1}$ is calculated by taking the following steps:

(i) Choose two sequences s_1 and s_2 from Eqs. (B1) and two types t_1 and t_2 that correspond to the two terms in Eq. (B2). Note that both the sequences and types may be the same, that is, $s_1 = s_2$ and/or $t_1 = t_2$ are allowed. This choice fully characterizes a particular contribution to the overall transition probability. In what follows, we will refer a particular choice (s,t) as a "process."

(ii) For a term of the first type (particle transport), choose a counterclockwise bubble [see, e.g., right bubble in Fig. 1(a)]. For a term of second type (hole transport), choose a clockwise bubble [see, e.g., right bubble in Fig. 1(b)]. Note that in Fig. 1 and in Eq. (26), τ_1 (τ_2), t (t'), and τ_3 (τ_4) are reserved for the pumping mode i, accepting mode f, and vibration v on the bubble corresponding to the first (second) process.

(iii) Draw a bubble representing the first process on the right and a bubble representing the second process on the left, and connect them by lines representing the Green's functions of the external optical fields and the vibration. The GF of the pumping mode i connects τ_1 and τ_2, that of the accepting mode f connects t and t', and the Green's function for the molecular vibration connects between τ_3 and τ_4. Note that under complex conjugation, the bubble of the second process changes its original direction (clockwise becomes counterclockwise and vice versa). The resulting diagrams (one of the four types presented in Fig. 1) has to be projected (see below) to get the expression corresponding to this contribution to the transition probability.

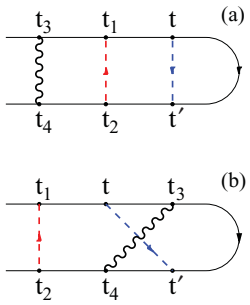

FIG. 6. (Color online) Examples of projections on the Keldysh contour.

(iv) On the upper (time-ordered) branch of the Keldysh contour, set the times in order of *the sequence* of events of the first process. On the lower (anti-time-ordering) branch of the Keldysh contour, set the times in order of *the sequence* of events of the second process (see Fig. 6). Connect the corresponding times by optical and vibration Green's function lines. This is the projection of the diagram obtained in the previous step. Note that t and t' are fixed.

(v) Taking the Fourier transforms of the resulting diagram projection yields the result of Ref. 30 for this contribution to the transition probability.

In what follows, we show some examples that illustrate this procedure.

Transition probability for electron transport via the Eq. (B1d) sequence. Here, the two processes are identical. Focusing on particle (electron) transport dictates choosing counterclockwise bubble for both processes. Drawing a conjugated (direction is reversed) bubble for the second process on the left and original (counterclockwise) bubble for the first process on the right (as in Fig. 1) and connecting times on the bubbles leads to the diagram shown in Fig. 1(a). Ordering the times on the Keldysh contour in accordance with the sequence (B1d) leads to projection shown in Fig. 6(a). The diagram projection will be

$$|U_i|^2|U_f|^2|M|^2 \int_{-\infty}^{+\infty} d(t-t')e^{i\nu_f(t-t')} \int_{-\infty}^{t} dt_1 \int_{-\infty}^{t'} dt_2 \times \int_{-\infty}^{t_1} dt_3 \int_{-\infty}^{t_2} dt_4\, \tilde{D}_i^{<}(t_1-t_2)\, D_v^{(0)<}(t_3-t_4) \times G^{(0)<}(t'-t_4)\, G^{(0)>}(t_4-t_2)\, G^{(0)>}(t_2-t') \times G^{(0)>}(t-t_1)\, G^{(0)>}(t_1-t_3)\, G^{(0)<}(t_3-t). \quad \text{(B4)}$$

Note that Ref. 30 considers the zero-temperature situation only, i.e., $N_v = 0$.

After Fourier transform and evaluation of the integrals one gets[52]

$$-2\pi\delta(\nu_f+\omega_v-\nu_i)|U_i|^2|U_f|^2|M|^2 \times \left| \int_{-\infty}^{+\infty} \frac{dE_1}{2\pi} \int_{-\infty}^{+\infty} \frac{dE_2}{2\pi} \int_{-\infty}^{+\infty} \frac{dE_3}{2\pi} \times \frac{G^{(0)<}(E_1)\, G^{(0)>}(E_2)\, G^{(0)>}(E_3)}{[E_2-E_1-\nu_f-i\delta][E_3-E_1+\omega_v-i\delta]} \right|^2, \quad \text{(B5)}$$

which is a generalization of the contribution to the Raman flux that arises from the sequence represented by the last term of Eq. (14) of Ref. 30 of the type represented by the first term in Eq. (15) of that paper.

Interference between electron and hole transport via the Eq. (B1d) sequence. Here, the two processes are different by type of transport, while they share the same sequence of events. A different type of transport for the first process dictates choosing opposite (clockwise) bubble. As a result, one gets the diagram shown in Fig. 1(d). Since the sequence is the same as in the previous example, the projection is still given by Fig. 6(a). This result comes from the same sequence [last term in Eq. (14) of Ref. 30], but interference between the two types [two terms in Eq. (15) of Ref. 30] is considered. Writing down the diagram projection and evaluating integrals is done in complete analogy with the previous case.

Interference between hole transport via the Eq. (B1f) sequence and electron transport via the Eq. (B1b) sequence. Here, both sequences and types of the processes are different. Making appropriate choices, one gets diagram shown in Fig. 1(a). Sequences of the process are ordered on the Keldysh contour as shown in Fig. 6(b). The diagram projection will be

$$|U_i|^2|U_f|^2|M|^2\int_{-\infty}^{+\infty}d(t-t')e^{i\nu_f(t-t')}\int_{-\infty}^{t}dt_1\int_{-\infty}^{t'}dt_4 \times\int_{t}^{+\infty}dt_3\int_{-\infty}^{t_4}dt_2\,\tilde{D}_i^{<}(t_1-t_2)\,D_v^{(0)<}(t_3-t_4) \times G^{(0)<}(t'-t_4)\,G^{(0)<}(t_4-t_2)\,G^{(0)>}(t_2-t') \times G^{(0)>}(t-t_1)\,G^{(0)<}(t_1-t_3)\,G^{(0)>}(t_3-t). \quad \text{(B6)}$$

Evaluation of the integrals is straightforward. The result corresponds to contribution to the total transition probability coming from the first and fourth terms in Eq. (14) of Ref. 30 of the type that corresponds to the second and first terms in Eq. (15), respectively, of that paper.

It is easy to see that the nonequilibrium version of the model of Ref. 30, obtained from the formalism of Sec. IV in the lowest order of electron-vibration interaction, and disregarding anti-Stokes processes (valid at low T), is obtained from the results of Ref. 30 by the following substitutions:

$$\int_{-\infty}^{E_F}dE\,\rho_0(E)\ldots\to -i\int_{-\infty}^{+\infty}\frac{dE}{2\pi}\,G^{(0)<}(E)\ldots, \quad \text{(B7)}$$

$$\int_{E_F}^{+\infty}dE\,\rho_0(E)\ldots\to \quad i\int_{-\infty}^{+\infty}\frac{dE}{2\pi}\,G^{(0)>}(E)\ldots. \quad \text{(B8)}$$

This becomes an identity at $T=0$ and equilibrium. Explicitly, this results in expressions (34)–(38) for the scattering flux. This approach allows us to get the Stokes signal at nonequilibrium with reasonable accuracy. For a more general description, one has to follow the self-consistent procedure of Eqs. (41) and (42), and use the resulting full Green's functions in projections of Eq. (26).

*michalo2@post.tau.ac.il
†migalperin@ucsd.edu
‡nitzan@post.tau.ac.il

[1] J. Zhang, Y. Fu, M. H. Chowdhury, and J. R. Lakowicz, Nano Lett. **7**, 2101 (2007).
[2] S. Nie and S. R. Emory, Science **275**, 1102 (1997).
[3] D. R. Ward, N. K. Grady, C. S. Levin, N. J. Halas, Y. Wu, P. Nordlander, and D. Natelson, Nano Lett. **7**, 1396 (2007).
[4] S. W. Wu, G. V. Nazin, and W. Ho, Phys. Rev. B **77**, 205430 (2008).
[5] D. R. Ward, N. J. Halas, J. W. Ciszek, J. M. Tour, Y. Wu, P. Nordlander, and D. Natelson, Nano Lett. **8**, 919 (2008).
[6] Z. Ioffe, T. Shamai, A. Ophir, G. Noy, I. Yutsis, K. Kfir, O. Cheshnovsky, and Y. Selzer, Nat. Nanotechnol. **3**, 727 (2008).
[7] N. Agrait, C. Untiedt, G. Rubio-Bollinger, and S. Vieira, Phys. Rev. Lett. **88**, 216803 (2002).
[8] N. B. Zhitenev, H. Meng, and Z. Bao, Phys. Rev. Lett. **88**, 226801 (2002).
[9] W. Wang, T. Lee, I. Kretzschmar, and M. A. Reed, Nano Lett. **4**, 643 (2004).
[10] D. R. Ward, D. A. Corley, J. M. Tour, and D. Natelson, Nat. Nanotechnol. **6**, 33 (2011).
[11] M. Galperin and A. Nitzan, Phys. Rev. Lett. **95**, 206802 (2005).
[12] M. Galperin and A. Nitzan, J. Chem. Phys. **124**, 234709 (2006).
[13] U. Harbola, J. B. Maddox, and S. Mukamel, Phys. Rev. B **73**, 075211 (2006).
[14] M. Galperin and S. Tretiak, J. Chem. Phys. **128**, 124705 (2008).
[15] M. Sukharev and M. Galperin, Phys. Rev. B **81**, 165307 (2010).
[16] S. Kohler, S. Camalet, M. Strass, J. Lehmann, G.-L. Ingold, and P. Hnggi, Chem. Phys. **296**, 243 (2004).
[17] M. Galperin, A. Nitzan, and M. A. Ratner, Phys. Rev. Lett. **96**, 166803 (2006).
[18] J. K. Viljas, F. Pauly, and J. C. Cuevas, Phys. Rev. B **76**, 033403 (2007).
[19] J. K. Viljas, F. Pauly, and J. C. Cuevas, Phys. Rev. B **77**, 155119 (2008).
[20] M. Galperin, M. A. Ratner, and A. Nitzan, Nano Lett. **9**, 758 (2009).
[21] M. Galperin, M. A. Ratner, and A. Nitzan, J. Chem. Phys. **130**, 144109 (2009).
[22] J. I. Gersten, R. L. Birke, and J. R. Lombardi, Phys. Rev. Lett. **43**, 147 (1979).
[23] A. Otto, Indian J. Phys. B **77**, 63 (2003).
[24] A. Otto and M. Futamata, *Surface-Enhanced Raman Scattering: Physics and Applications*, Topics in Applied Physics, Vol. 103 (Springer, Berlin, 2006), pp. 143–182.
[25] D. P. Fromm, A. Sundaramurthy, A. Kinkhabwala, P. J. Schuck, G. S. Kino, and W. E. Moerner, J. Chem. Phys. **124**, 061101 (2006).
[26] L. Cui, D.-Y. Wu, A. Wang, B. Ren, and Z.-Q. Tian, J. Phys. Chem. C **114**, 16588 (2010).
[27] J. R. Lombardi and R. L. Birke, Acc. Chem. Res. **42**, 734 (2009).
[28] S. M. Morton and L. Jensen, J. Am. Chem. Soc. **131**, 4090 (2009).
[29] S. M. Morton, D. W. Silverstein, and L. Jensen, Chem. Rev. **111**, 3962 (2011).

[30]B. N. J. Persson, Chem. Phys. Lett. **82**, 561 (1981).
[31]D. M. Newns, Phys. Rev. **178**, 1123 (1969).
[32]B. D. Fainberg, M. Sukharev, T.-H. Park, and M. Galperin, Phys. Rev. B **83**, 205425 (2011).
[33]B. Fainberg, V. Gorbunov, and S. Lin, Chem. Phys. **307**, 77 (2004).
[34]See, e.g., D. A. Long, *Raman Spectroscopy* (McGraw Hill, New York, 1977).
[35]A. P. Jauho, N. S. Wingreen, and Y. Meir, Phys. Rev. B **50**, 5528 (1994).
[36]J. D. Jackson, *Classical Electrodynamics* (Wiley, New York, 1998).
[37]This function is denoted $G(\omega,\omega \pm \omega_v)$ in Ref. 30.
[38]B. N. J. Persson, K. Zhao, and Z. Zhang, Phys. Rev. Lett. **96**, 207401 (2006).
[39]H. Schoeller, Lect. Notes Phys. **544**, 137 (2000).
[40]G. D. Mahan, *Many-Particle Physics* (Plenum, New York, 1990).
[41]H. Haug and A.-P. Jauho, *Quantum Kinetics in Transport and Optics of Semiconductors* (Springer, Berlin, 1996).
[42]Note that Eq. (35) differs from Eq. (13) of Ref. 30 by the absence of the vibrational operator $\hat{Q}$. Indeed, in (34), H refers to a matrix element between initial and final states which should not contain this operator but its matrix element between the ground and first excited oscillator states, which is unity in our reduced units.
[43]M. Galperin, M. A. Ratner, and A. Nitzan, J. Chem. Phys. **121**, 11965 (2004).
[44]A. Mitra, I. Aleiner, and A. J. Millis, Phys. Rev. B **69**, 245302 (2004).
[45]M. Galperin, A. Nitzan, and M. A. Ratner, Phys. Rev. B **73**, 045314 (2006).
[46]T.-H. Park and M. Galperin, Europhys. Lett. **95**, 27001 (2011).
[47]T.-H. Park and M. Galperin, Phys. Rev. B **84**, 075447 (2011).
[48]M. Galperin, K. Saito, A. V. Balatsky, and A. Nitzan, Phys. Rev. B **80**, 115427 (2009).
[49]M. Galperin and A. Nitzan, J. Phys. Chem. Lett. **2**, 2110 (2011).
[50]M. Galperin and A. Nitzan, Phys. Rev. B **84**, 195325 (2011).
[51]A. L. Fetter and J. D. Walecka, *Quantum Theory of Many-Particle Systems* (McGraw-Hill, New York, 1971).
[52]The minus sign in Eq. (B5) indicates that photon flux leaves the molecular system.